Prediction and Measurement of Direct Combustion Noise in Turbopropulsion Systems

D. C. Mathews* and N. F. Rekos Jr.†
Pratt & Whitney Aircraft, East Hartford, Conn.

The development of an improved prediction system for direct combustion noise is discussed. Expressions for acoustic power level, peak frequency, and full-scale engine acoustic transmission loss due to combustor/duct coupling and turbine attenuation are derived in terms of readily available performance and geometry parameters from the burner and turbine. New parameters introduced by the prediction system include the effects of fuel nozzle number and burner length. Predictions are in good agreement with noise data obtained from component rig tests on several JT8D burner configurations, and full-scale turbofan engines. The applicability of the system to the prediction of combustion noise levels, spectra, and directivity from full-scale engines is demonstrated for four P&WA turbofan engines; i.e., the JT8D-109, JT9D-7A, JT9D-70, and the prototype JT10D.

Nomenclature

A = cross-sectional area, in.^{2}
c = velocity of sound
C_1 = constant defined in Eq. (3)
c_p = specific heat at constant pressure (0.28 Btu/lb$_m$ °R in typical reaction region)
D = outer diameter of turbine at combustor/turbine interface, ft
F = ratio of characteristic impedances across turbine, Eq. (38)
F_b = burner fuel-air ratio
F_{st} = stoichiometric fuel-air ratio ≃0.068 for jet fuel and air
f_c = combustion noise peak frequency, Hz
H_f = fuel heating value ≅ 18,500 Btu/lbm for jet fuel
K_1, K_2, K_3 = constants defined in Eqs. (10), (27), and (28), respectively
K_f = constant in peak frequency model, Eq. (11)
L = length defined in Fig. 2, ft.
L_b = burner length, ft
L_r = length of reaction region in burner, ft
m = circumferential lobe number for spinning modes
N_f = number of fuel nozzles in burner
P = acoustic power
p_0' = acoustic pressure amplitude at burner exit
p = mean pressure, psia
$\dot{Q}$ = volumetric heat release rate, Btu/sec-ft^3
R = gas constant ≅ 53.35 ft-lb$_f$/lb$_m$ °R for air
R_w = defined in Eq. (20) and Ref. 3
r = distance from source to observer, ft
T = temperature, °R
T.L. = combustion noise transmission loss, dB
U_r = mean velocity through reaction region, fps
V = volume
w_{a_b} = burner airflow, lbm/sec
w_{a_r} = airflow through reaction region, lbm/sec
w_f = fuel flow rate, lb/sec
γ = ratio of specific heats
ρ = density
τ_r = typical reaction time, Eq. (4), sec.

Subscripts

4 = burner entrance location
5 = burner exit, turbine inlet location
7 = turbine exit location
∞ = denotes ambient conditions
b = denotes burner
corr = denotes correlated volume, area, etc.
d = duct
ref = burner reference (or design) condition
st = denotes stoichiometric condition
t = denotes stagnation value of pressure or temperature

Presented as Paper 76-579 at the 3rd AIAA Aero-Acoustics Conference, Palo Alto, Calif., July 20-23, 1976; submitted Sept. 2, 1976; revision received Jan. 18, 1977.
Index category: Noise.

*Assistant Project Engineer. Member AIAA.
†Analytical Engineer.

I. Introduction

Background

OF the several potential sources of core engine noise[1] from turbopropulsion systems, the dominant generation mechanisms currently are believed to be associated with the combustion process.[2-6] Recent studies at Pratt & Whitney Aircraft, conducted on a JT8D-109 turbofan engine,[7,8] have demonstrated (using signal cross-correlation techniques) that, over a wide variety of engine operating conditions, a substantial portion of the low frequency noise measured in the far field of the engine is generated by the combustor. Combustion generated noise is either of the "direct" type (i.e., resulting directly from the unsteady combustion) or of the "indirect" type,[9,10] which results from the convection of burner generated temperature fluctuations through the large pressure drop across the turbine. The current paper deals only with direct combustion noise, whereas a more detailed description of recent analytical and experimental studies of both types of noise, conducted at Pratt & Whitney Aircraft under funding from the Federal Aviation Administration, is presented in Ref. 8.

Many procedures for predicting direct combustion noise levels have been proposed and were summarized in recent literature surveys published by Strahle,[11] Motsinger,[12] and Huff.[13] Most methods, however, are empirical and apply primarily to noise generated by open flames. In addition, the methods suggested for actual combustors fail to properly predict observed differences in noise levels from different burner geometries.

Although much work has been directed toward the prediction of combustion noise levels, no procedure is currently available that explains the observed differences in combustion noise peak frequency from different burner

geometries. As shown in Sec. III, these frequencies, although nearly invariant for a given burner when operated over a wide range of conditions, have been observed to range between 280 to 500 Hz, depending on the burner geometry.

Another area that must be considered in the prediction of combustion noise levels from actual engines is the transmission loss that occurs between the combustor and the engine far field. Very little currently is known regarding the magnitude of these losses, but published estimates range from very small values to losses in excess of 40 dB.

As discussed in the preceding, several shortcomings exist in the current procedures for predicting combustion noise levels, frequencies, and transmission losses. As part of FAA Contract No. DOT-FA75WA-3663, an improved procedure was developed and is presented in this paper, together with experimental verification of the method using rig and engine data.

Elements of Current Prediction System

The development of the prediction system was divided into three parts: the formulation of analytical models for peak frequency, acoustic power level, and transmission loss; the verification of these models; and the development of empirical spectra and directivity patterns. The elements of the prediction system are summarized briefly below and described in the following sections.

Peak Frequency Model

An expression for peak frequency is derived and experimentally verified using far-field combustion noise data from both burner rigs and full-scale engines.

Acoustic Power Level Model

Starting with the solution to the nonconvective wave equation presented by Strahle[11] for the far-field sound from open flames, an expression is derived for the acoustic power levels generated by engine-type combustors, in terms of burner geometry and performance parameters. Variations in power level predicted by each term in the expression are verified independently using far-field combustion noise data from both rigs and full-scale engines.

Transmission Loss Model

An analytical expression is derived for the transmission losses associated with the combustor/duct coupling at the turbine entrance location and across the turbine itself. Empirical methods are used to establish necessary constants and experimental verification is presented, using comparisons of isolated burner rig and full-scale engine data.

Combustion Noise Directivity

The combustion noise directivity pattern used in the prediction system is obtained empirically from far-field engine noise data.

Combustion Noise Spectral Shape

Although the combustion noise peak frequency varies with burner geometry and is predicted by the peak frequency model, the spectral shape is determined empirically from burner rig and engine data.

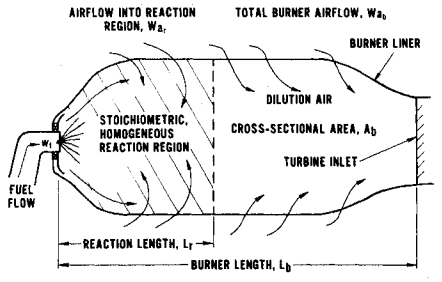

Fig. 1 Representation of reaction region in a burner.

II. Analytical Model Development

Representation of Reaction Region in a Burner

The reaction region inside a typical burner is approximated as shown in Fig. 1. The fuel flow w_f is introduced through one or more fuel nozzles, and the total airflow w_{a_b} is divided between that needed for the reactions w_{a_r} and that used as dilution air. The reaction length L_r is defined as the length of the region in which all of the fuel is totally burned. In the actual reaction region, burning takes place in a highly turbulent, recirculating flow environment. Since an exact representation of this flow is not available, the reaction region is approximated by a region within which the flow and thermodynamic properties are assumed to be spatially homogeneous. The reaction region, which will vary in size as the burner operating condition is changed, also is assumed to contain a fuel and air mixture that results in stoichiometric burning throughout. Thus, the following relationship exists between the reaction air and fuel flow rates:

$$w_{a_r} = w_f / F_{st} \tag{1}$$

where F_{st} is the stoichiometric fuel-air ratio. Remaining parameters required in the subsequent analytical model development include the burner fuel-air ratio, defined as

$$F_b = w_f / w_{a_b} \tag{2}$$

the burner cross-sectional area A_b, and burner length L_b. With these definitions and assumptions regarding the reaction region, the analytical models for combustion noise peak frequency and acoustic power level now may be presented.

Peak Frequency Model

Since the chemistry within the reaction region of a given burner is assumed to be invariant over all operating conditions (i.e., stoichiometric), the associated reaction time also are assumed to be independent of the burner operating condition, and therefore invariant for a specific burner. If we characterize the burning process by a typical reaction time scale τ_r, then the peak frequency of combustion noise (denoted by f_c) generated by these reactions should be inversely proportional to the values of τ_r (e.g., shorter reaction times result in higher frequencies). This may be expressed as follows:

$$f_c = C_1 / \tau_r \tag{3}$$

where C_1 is a constant, having the same value for all burners, and τ_r, as discussed in the preceding, may be different for different burners but is not a function of operation for a specific burner geometry. Thus the frequency predicted by Eq. (3) is a function only of burner geometry and not of burner performance. The validity of the assumptions leading to Eq. (3) is supported by the observations by several investigators[1-5,7] that, for a specified burner, the peak frequency of combustion generated noise remains essentially unchanged over wide ranges of operating conditions. In addition, the observed peak frequencies from different designs have been noted to vary from about 280 to 500 Hz, depending only on burner geometry.

An expression for the reaction time τ_r, appearing in Eq. (3), is derived next. Since all reactions occur within the length L_r (defined in Fig. 1), then a measure of the average time for these reactions to occur would be

$$\tau_r = L_r / U_r \tag{4}$$

where U_r is the mean flow velocity through the reacting region. The reaction time given in Eq. (4) is the average time that the air and fuel reside in the reaction region. A typical value of this residence time was calculated for several actual combustors to be about 0.002 sec, which is consistent with observed combustion noise frequencies in the 300-to 500-Hz

range. The frequency f_c now may be expressed as

$$f_c = C_1 (U_r / L_r) \tag{5}$$

The value of U_r at any operating condition can be described in terms of known parameters. Applying conservation of mass in the reaction region,

$$U_r = R w_{a_r} T_{st} / p_b A_b \tag{6}$$

where w_{a_r} is given by Eq. (1), p_b is the burner pressure, T_{st} is the stoichiometric temperature, and R is the gas constant. Since burner liner pressure drops usually are quite small, the burner pressure p_b can be approximated by the burner inlet total pressure p_{t_4}. In addition, from the energy equation, the stoichiometric temperature is

$$T_{st} = T_{t_4} (1 + H_f F_{st} / c_p T_{t_4}) \tag{7}$$

Realizing that the second term in the brackets of Eq. (7) is much larger than unity for typical values of T_{t_4}, Eq. (5) now may be written

$$f_c = C_1 (R H_f / c_p A_b) (w_f / p_{t_4} L_r) \tag{8}$$

Since, as shown earlier, f_c is not a function of burner operation, the last term in Eq. (8) must be a constant. Consider, then, a "reference" operating condition, which is chosen as the design point for the burner (usually near the aircraft takeoff condition). The peak frequency from Eq. (8) now may be written

$$f_c = C_1 (R H_f / c_p A_b) (w_f / p_{t_4} L_r)_{ref} \tag{9}$$

Next it is assumed that, at the reference (or design) condition, the design philosophy for a given type of burner (e.g., can-type, annular, etc.) is such that the reaction length is a constant fraction of the burner length (i.e., longer burners of a given type have proportionally longer reaction regions, etc.). Thus,

$$(L_r)_{ref} = K_1 L_b \tag{10}$$

where K_1 is a function only of burner type. Substituting Eq. (10) into (9) yields the final expression for combustion noise peak frequency,

$$f_c = K_f \frac{R H_f}{c_p} \left(\frac{w_f}{p_{t_4}} \right)_{ref} \frac{1}{A_b L_b} \tag{11}$$

where the proportionality constant K_f is given by

$$K_f = C_1 / K_1 \tag{12}$$

and is dependent only on burner type (e.g., can-type, annular, etc.).

It is interesting to note that, for a given ratio of fuel flow to burner pressure at the reference condition, the frequencies predicted by Eq. (11) are inversely proportional to the burner volume $A_b L_b$. Thus, for example, if engine design constraints resulted in a requirement for a shorter burner, keeping burner type and all other parameters constant, higher combustion noise frequencies should be expected. The validity of Eq. (11) is demonstrated in Sec. IV, where the value of K_f is shown to be about 8 for several can-type burners and 3 for annular burners.

Acoustic Power Level Model

Published theoretical studies of combustion noise deal with open turbulent flames. An approach developed by Strahle,[14] based upon Lighthill's equation, was expected to be valid for low-Mach-number flames. The low-Mach-number condition often prevails in typical aircraft-type combustors. Alternatively, the theory developed by Chiu and Summerfield[15] claims to include convection effects and results in an expression for far-field noise intensity which is more complex than that of Ref. 14. A current controversy exists over the reasons why the theories of Refs. 14 and 15 do not agree with each other in the same limit of low-Mach-number flows, however. Practically, the radiation emission results of Refs. 16 and 17 support the simpler theory as adequate, especially in view of the success in application to noise results from several flame types.[11] Consequently, the Strahle model will be employed. The Strahle model results in an expression for far-field noise from an open flame (source assumed to be compact) in terms of the volume integral of the time derivative of the heat release rate (volumetric) in the combustion region, i.e.,

$$p'(r,t) = \frac{\gamma - 1}{4\pi r c_\infty^2} \int_{V(r_0)} \frac{\partial}{\partial t} \dot{Q}\left(r_0, t - \frac{r}{c_\infty}\right) dV(r_0) \tag{13}$$

where r is the distance from the center of the reaction region to the observation point in the far-field, r_0 is the vector from the center of the reaction region to the volume element $dV(r_0)$, and $\dot{Q}$ is the volumetric heat release rate.

If the source is correlated over a known volume, then $\partial \dot{Q} / \partial t$ is the same at all points within this volume, and Eq. (13) can be written

$$p'(r,t) = \frac{\gamma - 1}{4\pi r c_\infty^2} \left(\frac{\partial \dot{Q}}{\partial t} \right)_{t - r/c_\infty} V_{corr} \tag{14}$$

where V_{corr} is the volume of the correlated reaction region producing the noise. The acoustic power level from this source may be written

$$P = (< p'^2 > / \rho_\infty c_\infty)(4\pi r^2) \tag{15}$$

Upon substituting Eq. (14) into (15), the power becomes

$$P = \frac{(\gamma - 1)^2}{4\pi \rho_\infty c_\infty^5} < \left(\frac{\partial \dot{Q}}{\partial t} \right)^2 > V_{corr}^2 \tag{16}$$

Consider now an array of N such sources, each independent and uncorrelated with all others. Then the total power from these sources is

$$P_{tot} = N \frac{(\gamma - 1)^2}{4\pi \rho_\infty c_\infty^5} < \left(\frac{\partial \dot{Q}}{\partial t} \right)^2 > V_{corr}^2 \tag{17}$$

Considering the noise-producing fluctuations in $\dot{Q}$ at the peak frequency of radiated noise f_c, the mean square term in Eq. (17) can be represented as follows:

$$< (\partial \dot{Q} / \partial t)^2 > \propto f_c^2 < \dot{Q}'^2 > \tag{18}$$

where $< \dot{Q}'^2 >$ is the mean square amplitude of the fluctuations in $\dot{Q}$. The total power now can be written

$$P_{tot} \propto [(\gamma - 1)^2 / 4\pi \rho_\infty c_\infty^5] N f_c^2 V_{corr}^2 < \dot{Q}'^2 > \tag{19}$$

Equation (19) is applicable to noise from open flames. Strahle[3] has derived the following expression, which relates the noise from a ducted source to that from an open source:

$$P_{duct} = P_{open} / R_w \tag{20}$$

where R_w is given in Ref. 3 as a function of frequency and the acoustic impedances of the burner liner walls and exit plane. Therefore, using Eqs. (19) and (20), the expression for combustion noise from N ducted sources in an engine burner

may be written as

$$P_{\text{comb}} \propto \frac{1}{R_w} \frac{(\gamma-1)^2}{4\pi\rho_\infty c_\infty^5} N f_c^2 V_{\text{corr}}^2 <\dot{Q}'^2> \tag{21}$$

Next it is assumed that in an actual combustor, the correlation volume V_{corr} is represented by the volume of the reaction region downstream of each fuel nozzle. Thus, the number of sources N is equal to the total number of fuel nozzles N_f in a given combustor, and the correlation volume may be written as

$$V_{\text{corr}} = A_b L_r / N_f \tag{22}$$

The combustion noise acoustic power then is

$$P_{\text{comb}} \propto \left[\frac{1}{R_w} \frac{(\gamma-1)^2}{4\pi\rho_\infty c_\infty^5} \frac{1}{N_f} f_c^2 A_b^2 L_r^2 <\dot{Q}'^2> \right] \tag{23}$$

From the general expression for peak frequency [i.e., from Eqs. (5-7)], f_c may be written as

$$f_c \propto \frac{R w_{a_b} T_{t_4}}{p_{t_4} A_b L_r} \frac{F_b}{F_{\text{st}}} \left(1 + \frac{H_f F_{\text{st}}}{c_p T_{t_4}}\right) \tag{24}$$

Substituting Eq. (24) into (23) and rearranging in terms of independent burner performance and geometry parameters yields

$$P_{\text{comb}} \propto \left[\frac{(\gamma-1)^2 R^2}{R_w 4\pi\rho_\infty c_\infty^5 F_{\text{st}}^2} \frac{1}{N_f} A_b^2 p_{t_4}^2 \times \left(\frac{w_{a_b}\sqrt{T_{t_4}}}{p_{t_4} A_b}\right)^4 \left(1 + \frac{H_f F_{\text{st}}}{c_p T_{t_4}}\right)^2 F_b^2 \left(\frac{<\dot{Q}'^2> A_b^2}{w_{a_b}^2}\right) \right] \tag{25}$$

The last term in Eq. (25) contains the mean square fluctuation in volumetric heat release rate. It is assumed that this term is constant, i.e.,

$$\dot{Q}' \propto w_{a_b} / A_b \tag{26}$$

which requires that the fluctuating heat release rate (per unit volume) be proportional to the mean airflow (per unit area) through the burner. The validity of this assumption is examined in Sec. IV, where predictions from Eq. (25) which use this assumption are shown to agree with experimental data. Substituting Eq. (26) into (25), and combining all constant terms, the final expression for the combustion noise acoustic power results;

$$P_{\text{comb}} = K_2 \left[\frac{1}{N_f} A_b^2 p_{t_4}^2 \left(\frac{w_{a_b}\sqrt{T_{t_4}}}{p_{t_4} A_b}\right)^4 \left(1 + \frac{H_f F_{\text{st}}}{c_p T_{t_4}}\right)^2 F_b^2 \right] \tag{27}$$

where the proportionality constant K_2 may be a function of the fuel and oxidizer type, burner liner and exit impedances, and details of the burner geometry which have not been accounted for specifically in the analysis. The value of this constant must be determined by experiment. The next two terms in Eq. (27) contain burner geometry information, including the predicted result that the combustion noise power is inversely proportional to the number of fuel injection sources (fuel nozzles) in the burner. The final four terms in Eq. (27) involve four independent burner performance parameters (i.e., the burner pressure, p_{t_4}, burner flow parameter, normalized burner inlet temperature, and the burner fuel-air ratio F_b). Other performance parameters may be expressed in terms of these four independent parameters.

The acoustic power level, or OAPWL (in decibels) obtained from Eq. (27), may be written as

$$\text{OAPWL} = 10 \log\left[\frac{1}{N_f} A_b^2 p_{t_4}^2 \left(\frac{w_{a_b}\sqrt{T_{t_4}}}{p_{t_4} A_b}\right)^4 \times \left(1 + \frac{H_f F_{\text{st}}}{c_p T_{t_4}}\right)^2 F_b^2 \right] + K_3 \sim \text{dB} \quad (\text{ref.} 10^{-12}\text{W}) \tag{28}$$

where $K_3 = 10 \log K_2$, and must be determined from experiment. A detailed, term-by-term experimental verification of the predictions from Eq. (28) is presented in Sec. IV, where K_3 is shown to equal 132.

Transmission Loss Model

In the following discussion, an analytical model is presented which relates the noise generated by an isolated combustor to that generated by a combustor installed in an engine. This model accounts for the transmission losses associated with combustor/duct coupling at the turbine entrance location, and also across the turbine itself. Experimental verification of the model is presented in Sec. IV.

Transmission Loss Due to Combustor/Duct Coupling

The duct at the combustor/turbine interface has a specified outer diameter D, as shown in Fig. 2a. The area over which the combustion noise pressure fluctuations are correlated at this interface is given by

$$A_{\text{corr}} = (L/\pi D) A_{\text{duct}} \tag{29}$$

where L is the circumferential correlation length at the interface (shown in Fig. 2a) and A_{duct} is the total cross-sectional area of the annular duct. It is assumed that, over the low-frequency range of interest, the sound power radiated from an isolated combustor is carried by plane waves in the burner and may be expressed by

$$P_b = (p_0'^2 / 2\rho_5 c_5) A_{\text{corr}} \tag{30}$$

where p_0' is the acoustic pressure amplitude at the burner exit plane (station 5). This relationship has been verified experimentally[8] where it is shown that, for several JT8D-type burners tested separately in a rig at atmospheric pressure, the sound powers calculated from Eq. (30), using the isolated combustor rig exit area as the correlated area, agree quite well with the sound powers obtained from far-field noise measurements.

Next it is assumed that, when the combustor is installed in an annular duct, the acoustic pressure at the combustor/duct interface has the same amplitude as it would have at the exit of the isolated combustor operating at the same condition. This is equivalent to stating that the acoustic pressure at the interface is independent of any downstream acoustic impedance. The acoustic particle velocity, however, may vary at the combustor exit depending on the downstream installation, resulting in differences in the radiated sound power.

The final assumption deals with the modal distribution of the noise in the duct downstream of the burner. Here, the acoustic energy from each correlated source is assumed to be

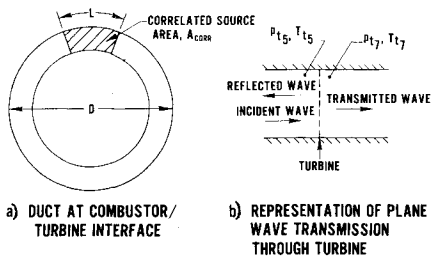

Fig. 2 Elements of combustion noise transmission loss model.

carried in the duct plane wave mode only. Calculations for several engines indicate that, in the combustion noise frequency range, the higher-order modes can be neglected, since they decay in the exhaust duct and therefore do not propagate acoustic energy. The acoustic pressure amplitude of the duct plane wave mode is obtained by modeling the circumferential acoustic pressure distribution as a pulse of circumferential length L and amplitude p'_0. The Fourier decomposition of this spatial pulse gives the following expression for the amplitude of the $m=0$ (i.e., plane wave) duct mode:

$$p'_{m=0} = (L/\pi D)\, p_0'^2 \tag{31}$$

The intensity of the plane wave mode in the duct is then

$$I_{m=0} = \frac{(L/\pi D)^2 p_0'^2}{2\rho_5 c_5} \tag{32}$$

and the acoustic power radiated from the ducted source is

$$P_d = \frac{(L/\pi D)^2 p_0'^2}{2\rho_5 c_5} A_{\text{duct}} \tag{33}$$

The transmission loss associated with the combustor/duct coupling can be expressed (in decibels) in terms of the ratio of power generated by the isolated burner to the power generated by the same burner coupled with a duct, i.e.,

$$(\text{T.L.})_d = 10\log(P_b/P_d) \tag{34}$$

which, from Eqs. (30) and (33), becomes

$$(\text{T.L.})_d = 10\log\left[\frac{A_{\text{corr}}}{(L/\pi D)^2 A_{\text{duct}}}\right] \tag{35}$$

Substituting Eq. (29) into Eq. (35) yields

$$(\text{T.L.})_d = 10\log(L/\pi D)^{-1} \tag{36}$$

This energy loss occurs as a result of differences in acoustic particle velocity between the two cases of an isolated combustor and the ducted combustor, and is dependent only on the ratio of the correlated source area at the combustor exit to the total duct area at the combustor/turbine interface. Thus, as an example, if the source at the combustor exit is correlated over only 10% of the circumference (i.e., $L/\pi D=0.1$), a 10-dB transmission loss would be predicted using Eq. (36), whereas if the source were correlated over the entire duct, all of the energy is in the plane wave mode, and there would be no transmission loss. The value of $L/\pi D$ must be measured experimentally or established empirically using experimental data. An empirical estimate of this factor, based on rig and engine data, is presented in Sec. IV.

Turbine Transmission Loss

The transmission loss associated with a plane wave traveling through the turbine is obtained by representing the entire turbine as a surface of discontinuity in characteristic impedance ρc. This is depicted schematically in Fig. 2b, where the length of the turbine is assumed to be small relative to the acoustic wavelength of the incident noise. (For typical engines, the ratio of acoustic wavelength to turbine length is about 4). It is assumed also that no reflections occur from locations in the tailpipe downstream of the turbine. This assumption appears valid for most engine configurations, where noise carried by plane waves at typical combustion noise frequencies is totally transmitted at the exhaust nozzle exit. As the incident acoustic plane wave contacts the turbine, both reflected and transmitted plane waves are developed due to the difference in characteristic impedance across the turbine. If the axial flow through the turbine is neglected (i.e., low axial Mach numbers), the ratio of the incident to the transmitted power can be expressed (from Ref. 18) as

$$P_i/P_t = (1+F)^2/4F \tag{37}$$

where F is the ratio of the upstream characteristic impedance (at station 5) to the downstream (station 7) characteristic impedance. Since the axial Mach numbers are fairly low at both locations, the static pressures and temperatures may be approximated by the more readily available stagnation values, and F may be expressed by

$$F = (p_{t_5}/p_{t_7})\sqrt{T_{t_7}/T_{t_5}} \tag{38}$$

From Eq. (37), the transmission loss across the turbine (in decibels) is

$$(\text{T.L.})_{\text{turb}} = 10\log[(1+F)^2/4F] \sim \text{dB} \tag{39}$$

Typical values of F in an actual engine range from 3 to 8, resulting in a transmission loss calculated from Eq. (39) of approximately 1 to 4 dB.

Total Transmission Loss

The total transmission loss associated with both the combustor/duct coupling and the turbine may be expressed (in decibels) as

$$\text{T.L.} = (\text{T.L.})_d + (\text{T.L.})_{\text{turb}} \tag{40}$$

From Eqs. (36) and (39), this becomes

$$\text{T.L.} = 10\log[(1+F)^2/4F(L/\pi D)] \sim \text{dB} \tag{41}$$

It is interesting to note that, for the low frequencies assumed in the analysis, the total transmission loss is independent of frequency. Thus, the noise spectra radiated from isolated combustors should be similar to the noise spectra from combustors installed in engines. This indeed is the case, as

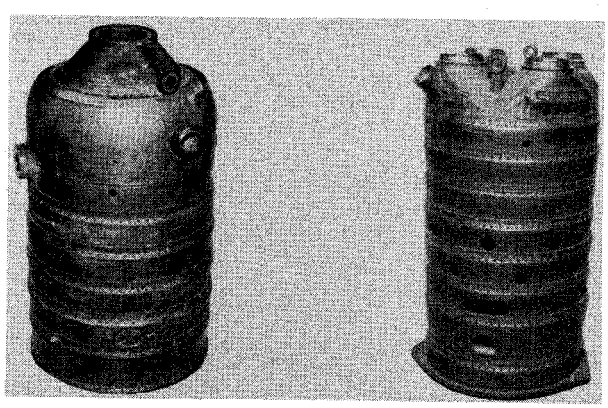

Fig. 3 JT8D-17 and J52 burners.

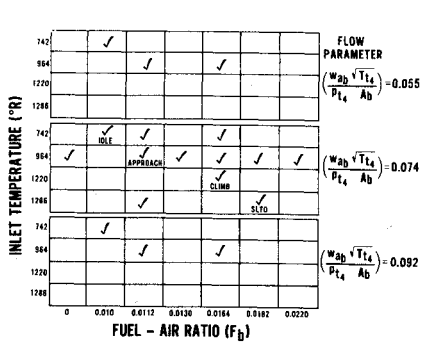

Fig. 4 JT8D burner rig test conditions.

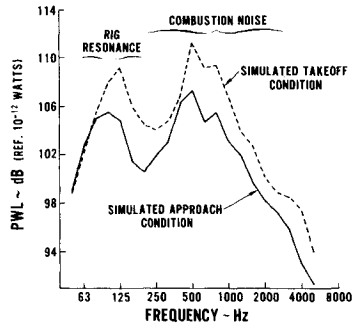

Fig. 5 Typical power level spectra for JT8D-9 burner.

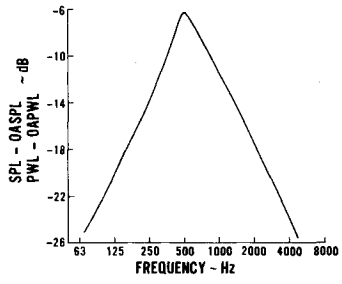

Fig. 6 Generalized combustion noise spectra for JT8D-type burners.

shown in the following section for the JT8D burner. The predictions of Eq. (41) are evaluated in Sec. IV.

III. Combustion Noise Experimental Data

In this section, a summary of data is presented from both JT8D burner rig combustion noise tests and full-scale engine tests. This discussion deals primarily with typical far-field spectra and directivities, whereas more complete details will be included in Sec. IV.

JT8D Burner Rig Test Program

One of the main objectives of the FAA sponsored JT8D rig test program was to identify the important characteristics of direct combustion noise and to aid in the evaluation of the direct combustion noise analytical model, including independent evaluations of the effects on combustion noise of variations in fuel-air ratio, inlet temperature, burner flow parameter, and number of fuel nozzles, using several different JT8D-type burner geometries.

Burner Configurations

Although six burner configurations were tested as part of the FAA program (including several low emissions designs), results from only three burners that best demonstrate the key burner noise characteristics are discussed in this paper. These include the JT8D-9 and JT8D-17 production burners, having single fuel nozzles, and a J52 (early turbojet version of JT8D) burner, of the same size, but having four fuel nozzles. Photographs of two of these burners are shown in Fig. 3. JT8D engines each contain nine of these can-type burners.

JT8D Burner Rig

Each JT8D-type burner was mounted in a rig that simulated a 40 degree (one-ninth) annular segment of an engine burner case, since only one can was being tested. At the burner exit location, an annular-to-round transition section and a round diffuser were added to minimize jet noise by maintaining jet velocities below 500 fps at all operating conditions. Performance parameters were monitored using arrays of pressure and temperature probes mounted upstream and downstream of the burner, and various fuel and airflow measurement devices.

Outdoor Combustion Noise Test Facility

Far-field noise data for each JT8D-type burner were obtained at a facility constructed specifically for combustion noise investigations. Microphones were located at a radial distance of 35 ft from the JT8D burner rig exit at 10 deg increments between 80 and 160 deg to the inlet axis. Noise data were obtained using microphones located ½-in. above a hard asphalt surface. Six dB were subtracted from the measured noise levels to obtain an estimate of free-field levels.

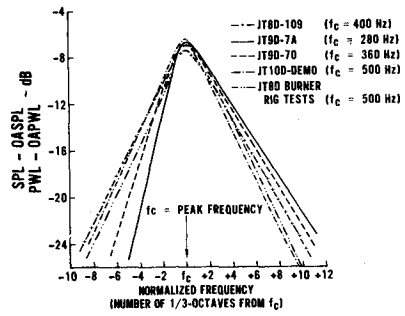

Fig. 7 Normalized combustion noise spectra.

Test Conditions

Eighteen test conditions were selected for each burner to investigate the effect of independent variations in inlet temperature, fuel-air ratio, and burner flow parameter on combustion noise. All burner performance variables can be related to these three independent parameters and the burner pressure. Since the JT8D burner rig exhausts to atmosphere, burner pressures were limited to values that resulted in noncontaminating levels of jet noise. This limit precluded study of the effect of pressure on combustion noise generation. The eighteen-point test matrix used in the program is shown in Fig. 4, and includes simulated engine idle, approach, climb, and takeoff conditions, together with 14 off-design burner operating conditions. The simulation is exact, except for burner pressure levels, limited as discussed previously.

Typical Test Results

Combustion noise was clearly evident in the measured spectra from each burner at all test conditions. Acoustic power level (PWL) spectra were obtained for each test condition by numerically integrating the sound pressure level (SPL) spectra over all far-field angles. Typical PWL spectra from the JT8D-9 burner at the simulated aircraft approach and takeoff test conditions are presented in Fig. 5. With few exceptions, the combustion noise peaked in the 500-Hz one-third octave band at all operating conditions and far-field measurement locations. (The 100-Hz noise peak shown in Fig. 5 was determined to be a burner rig resonance phenomenon.)

Investigation of many SPL and PWL spectra from all of the burners tested resulted in the generalized JT8D combustion noise spectral definition shown in Fig. 6. The overall acoustic power levels (OAPWL) from the three JT8D-type burners will be presented and discussed in Sec. IV.

Full-Scale Engine Data

Combustion noise spectral and directivity characteristics for several P&WA turbofan engines (i.e., the JT8D-109, JT9D-7A, JT9D-70, and the prototype JT10D) are presented in this section, whereas the overall acoustic power levels for these engines are discussed in Sec. IV. Noise data from these engines were obtained on P&WA's outdoor engine noise test stand described by McMahon.[19] Noise signals were recorded with ground-level microphones located at 10-deg increments between 90 and 150 deg to the inlet axis, at a radius of 150 ft from the engine exhaust plane.

Spectral Characteristics

The combustion noise spectral definitions for the four engines, obtained from detailed analysis of measured noise spectra, are presented in Fig. 7. The predicted jet noise characteristics were subtracted from the total spectra in this

analysis. The characteristics of engine combustion noise spectra are summarized here and discussed in more detail in Ref. 8.

1) The normalized combustion noise spectra from all four engines are similar, and agree well with the JT8D combustion noise spectra obtained from rig tests (Figs. 6 and 7).

2) The combustion noise peak frequency f_c is different for each engine.

3) For a given engine, the combustion noise peak frequency is essentially constant over the engine operating range, consistent with the results of the JT8D burner component tests, and with the predictions from the peak frequency model.

4) Combustion noise spectral characteristics are independent of far-field location.

Directivity Characteristics

The combustion noise directivity patterns obtained for the four P&WA turbofan engines are shown in Fig. 8. The curves shown for each engine represent the average directivity for several operating conditions.

IV. Experimental Verification of Analytical Models

Frequency Model

The expression derived for combustion noise peak frequency, Eq. (11), contains a proportionality constant K_f, which was stated to be dependent on burner type. Figure 9 plots measured values of f_c vs the right-hand side of Eq. (11), for both can-type and annular burners, using data from JT8D rig tests and five turbofan engines. The data for can-type burners are seen to fall along one line, and data for annular along another, as predicted by the model. Values of the constant K_f are seen to be 8 and 3, respectively, for can-type and annular burners. The trend toward higher frequencies for smaller volume burners is evident for the JT9D-7, JT9D-70, and JT10D-prototype engines. The "ref" condition (or design point) was taken to be takeoff power for the cases shown in Fig. 9.

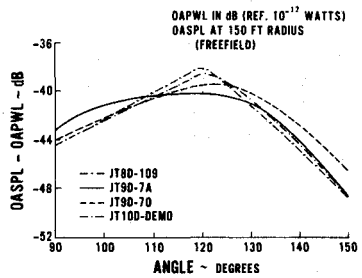

Fig. 8 Engine directivity characteristics.

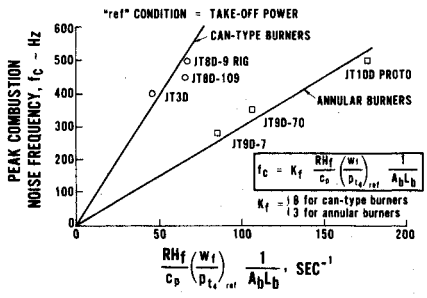

Fig. 9 Combustion noise peak frequency correlation.

The expression derived for combustion noise peak frequency, Eq. (11), contains a proportionality constant K_f, which was stated to be dependent on burner type. Figure 9 plots measured values of f_c vs the right-hand side of Eq. (11), for both can-type and annular burners, using data from JT8D rig tests and five turbofan engines. The data for can-type burners are seen to fall along one line, and data for annular along another, as predicted by the model. Values of the constant K_f are seen to be 8 and 3, respectively, for can-type and annular burners. The trend toward higher frequencies for smaller volume burners is evident for the JT9D-7, JT9D-70, and JT10D-prototype engines. The "ref" condition (or design point) was taken to be takeoff power for the cases shown in Fig. 9.

Acoustic Power Level Model

The predicted combustion noise OAPWL, as expressed by Eq. (28), is verified in the following discussion by comparing the predicted variation due to each term in the equation with the measured variation, using the combustion noise data discussed in the preceeding section.

Effect of Fuel/Air Ratio

Figure 10 presents combustion noise power levels from the isolated JT8D-9 burner as a function only of the burner fuel-air ratio F_b. Both the burner flow parameter and inlet temperature were held constant for this evaluation. Since, however, the burner pressure could not be varied independently to obtain desired values of the other parameters, the acoustic power levels in Fig. 10 have been normalized by the predicted influence of burner pressure. Since, however, the burner pressures varied only from 15.5 to 17.5 psia over the entire range of operation, this normalization is almost inconsequential. The slope of the data shown in Fig. 10 is seen to be in excellent agreement with the predicted influence of fuel-air ratio given in Eq. (28), where noise levels increase with the square of F_b.

Effect of Burner Flow Parameter

The independent effects of burner flow parameter on combustion noise from the JT8D-9 burner are shown in Fig. 11 for two cases of constant fuel-air ratio and inlet temperature. Again, the predicted dependence on flow parameter, from Eq. (28), is in good agreement with the slopes of both data sets.

Effect of Burner Inlet Temperature

Figure 12 shows the independent effects of burner inlet temperature on combustion noise from the three JT8D-type burners discussed in Sec. III, where fuel-air ratio and flow parameters were held constant. For standard jet fuel, the value of $H_f F_{st}/c_p$ is taken to be 4500°R. Although the experimental temperature varied only from 742° to 1220°R, the noise trends shown in Fig. 12 are in good agreement with the slopes predicted by Eq. (28). It should be noted that, as the burner inlet temperature is increased, keeping all other parameters constant, the combustion noise levels decrease.

Effect of Number of Fuel Nozzles

In order to verify the predicted effect of the number of fuel nozzles on combustion noise, the J52 four fuel nozzle burner was tested. Since this burner has the same cross-sectional area and length as the single fuel nozzle burners, Eq. (28) predicts that, at a given burner operating condition, the J52 burner

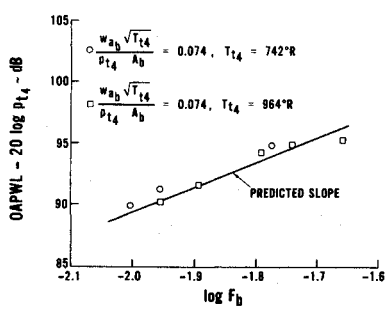

Fig. 10 Effect of fuel-air ratio variations on combustion noise levels (JT8D-9 burner).

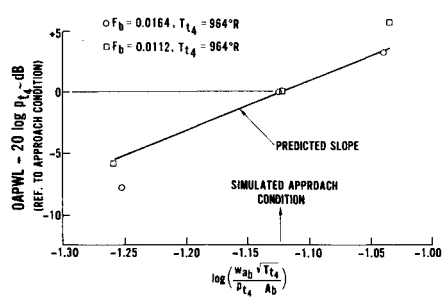

Fig. 11 Effect of burner flow parameter on combustion noise levels (JT8D-9 burner).

should be 6 dB quieter than the single fuel nozzle JT8D-17 burner. A comparison of combustion noise levels from the J52 and the JT8D-17 burners is shown in Fig. 13, where the noise is plotted as a function of the entire parameter of Eq. (28), except the term involving the number of fuel nozzles. The data from both burners are in agreement with the predicted slope from Eq. (28), and the expected 6-dB difference, due to the number of fuel nozzles, is evident.

When the predicted influence of fuel nozzle number is taken into account, the data shown in Fig. 13 collapse, as shown in Fig. 14. Here, the combustion noise correlation shown by the solid line is given by

$$\mathrm{OAPWL} = 10 \log\left[\frac{1}{N_f} A_b{}^2 p_{t_4}{}^2 \left(\frac{w_{a_b}\sqrt{T_{t_4}}}{p_{t_4} A_b}\right)^4 \times \left(1+\frac{H_f F_{st}}{c_p T_{t_4}}\right)^2 F_b{}^2\right] + 132 \sim \mathrm{dB}$$

$$(\text{ref. } 10^{-12}\mathrm{W}) \qquad (42)$$

where this is seen to be identical to Eq. (28), with the constant K_3 set equal to 132.

Effect of Burner Pressure

As mentioned previously, the independent effects of burner pressure could not be determined from the component JT8D rig tests. Since, however, the other terms in Eq. (28) have been experimentally verified using the rig data, the independent effects of pressure can be determined by normalizing the engine noise levels by everything but burner pressure (assuming the transmissions loss is not a strong function of engine operation) and presenting the normalized levels as a function of burner pressure. This is shown in Fig. 15, where the normalized combustion noise power levels from several turbofan engines are seen to increase with the square of burner pressure, as predicted in Eq. (28).

Acoustic Power Level Correlation

Combustion noise power levels from the JT8D-type combustors (including single fuel nozzle and four fuel nozzle designs) is presented in Fig. 16, together with the results from the four P&WA turbofan engines discussed in Sec. III. The data are presented as a function of the total power level parameter given in Eq. (28). The correlation line shown is the same as that presented in Fig. 14, and is given in Eq. (42). The acoustic power levels from the turbofan engines are seen in Fig. 16 to lie approximately 7 to 10 dB lower than the correlation line. This difference is attributable to the transmission loss, which is discussed next.

Transmission Loss Model

The expression for acoustic transmission loss, given in Eq. (41), includes the ratio $L/\pi D$, which represents the extent to which the acoustic pressures are circumferentially correlated in the engine at the combustor/turbine interface. The value of this ratio was determined empirically in the present study by requiring that the rig and engine data shown in Fig. 16 collapse when the engine data have been corrected for the transmission loss. This occurs when it is assumed that the source is correlated over 20% of the duct circumference at the combustor/duct interface (i.e., $L/\pi D = 0.2$) for can-type and annular burner installations. The results are shown in Fig. 17, where the final combustion noise correlation is shown by the straight line, and may be written as follows:

$$\mathrm{OAPWL} = 10 \log\left[\frac{1}{N_f} A_b{}^2 p_{t_4}{}^2 \left(\frac{w_{a_b}\sqrt{T_{t_4}}}{p_{t_4} A_b}\right)^4 \times \left(1+\frac{H_f F_{st}}{c_p T_{t_4}}\right)^2 F_b{}^2\right] + 132 - \mathrm{T.L.} \qquad (43)$$

where the transmission loss, T.L., is given in Eq. (41) with $L/\pi D = 0.2$.

V. Summary of Combustion Noise Prediction Procedure

Based on the analytical and experimental results presented in the preceding sections, a procedure was formulated which is applicable to the prediction of direct combustion noise power levels, directivity patterns, and spectral characteristics. The procedure is summarized in this section.

Combustion Noise Power Levels

The prediction of combustion noise power levels from full-scale engines must consider both the noise generation and the transmission losses associated with the combustor/duct

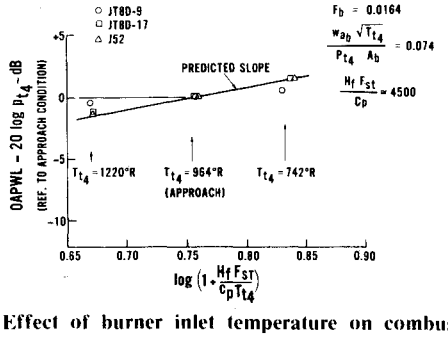

Fig. 12 Effect of burner inlet temperature on combustion noise levels.

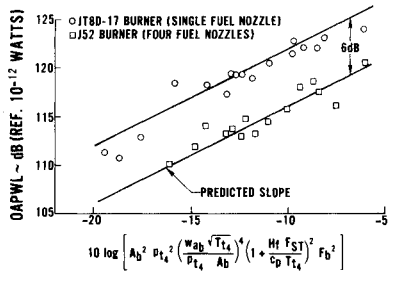

Fig. 13 Combustion noise level differences due to number of fuel nozzles.

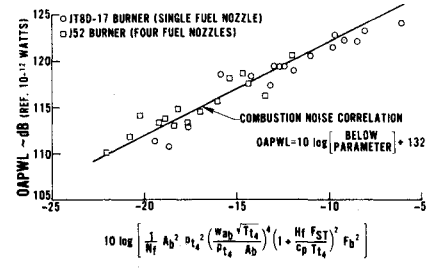

Fig. 14 Combustion noise correlation, including effect of fuel nozzle number.

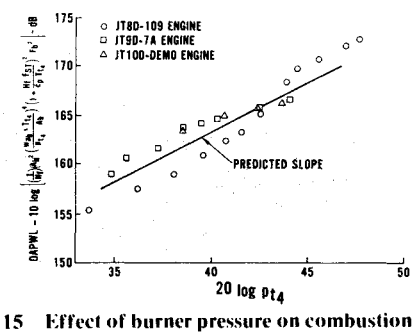

Fig. 15 Effect of burner pressure on combustion noise levels.

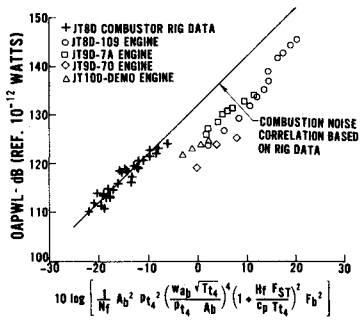

Fig. 16 Comparison of combustor rig and engine data.

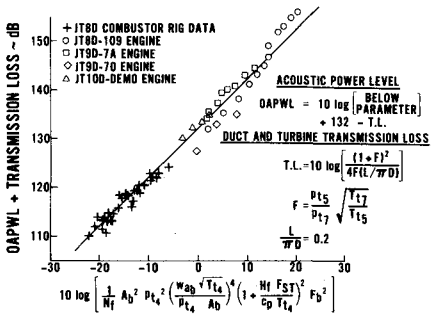

Fig. 17 Combustion noise acoustic power level correlation.

coupling and the turbine. A relationship has been derived which meets this requirement and also collapses the noise data from both burner rigs and full-scale engines, as shown in Fig. 17. For summary purposes, this relationship is rewritten as follows:

$$\mathrm{OAPWL} = 10\log\left[\frac{1}{N_f}A_b{}^2 p_{t_4}{}^2\left(\frac{w_{a_b}\sqrt{T_{t_4}}}{p_{t_4}A_b}\right)^4 \times\left(1+\frac{H_f F_{st}}{c_p T_{t_4}}\right)^2 F_b{}^2\right] + 132 - \mathrm{T.L.} \sim \mathrm{dB} \quad (43)$$

$(\mathrm{ref.}\,10^{-12}\,\mathrm{W})$

where

$$\mathrm{T.L.} = 10\log[(1+F)^2/4F(L/\pi D)] \sim \mathrm{dB} \quad (41)$$

F is the ratio of characteristic impedances across the turbine, given by

$$F = (p_{t5}/p_{t7})\sqrt{T_{t7}/T_{t5}} \quad (38)$$

and $L/\pi D = 0.2$ (obtained empirically). The data from both rigs and engines, shown in Fig. 17, fit the prediction of Eq. (43), with a standard deviation of 1.7 dB.

Combustion Noise Directivity

The directivity pattern presented in Fig. 18 is recommended for use in determining the overall sound pressure level (OASPL) of combustion noise as a function of angle from the inlet axis. This directivity was established empirically by averaging the characteristics presented in Fig. 8 for four P&WA turbofan engines. Although Fig. 18 applies at a radius of 150 ft from the engine, the values of free-field OASPL at any other distance may be determined using standard methods.

Combustion Noise Spectra

Based on an average of the combustion noise spectra from measured rig and engine data presented in Fig. 7, a generalized combustion noise one-third octave spectrum was

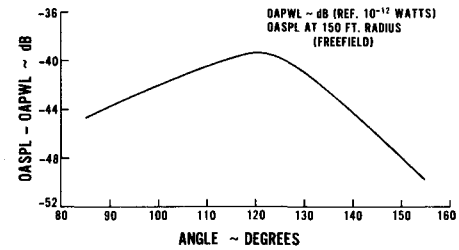

Fig. 18 Normalized combustion noise directivity.

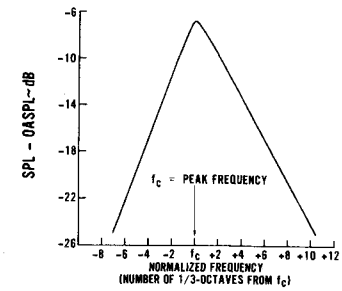

Fig. 19 Generalized combustion noise one-third-octave spectra.

obtained and is presented in Fig. 19. The maximum SPL from this spectrum is seen to be 6.8 dB below the OASPL. The frequency scale has been normalized in terms of the number of one-third octaves from the peak frequency f_c. For a given burner, the combustion noise spectrum is the same at all far-field angles and burner operating conditions. The peak frequency of combustion noise is, however, a function of burner geometry. The expression for peak frequency f_c is given by

$$f_c = K_f\frac{RH_f}{c_p}\left(\frac{w_f}{p_{t_4}}\right)_{\mathrm{ref}}\frac{1}{A_b L_b} \quad (11)$$

where $K_f = 8$ for can-type burners and $K_f = 3$ for annular burners. The reference (or design) condition, denoted by "ref," is taken to be at the engine takeoff power condition. The validity of the previous expression is demonstrated in Fig. 9.

VI. Conclusions

Results from the analytical and experimental studies presented in the preceding sections support the following conclusions.

Combustion Noise Power Levels

1) Predicted and measured combustion noise power levels are inversely proportional to the number of fuel nozzles in the burner, thus suggesting that an effective means of reducing combustion noise would be to increase the number of fuel nozzles.

2) Predicted and measured combustion noise power levels increase with both burner pressure and fuel-air ratio to a power of 2; increase with burner flow parameter to a power of 4; and decrease with increasing inlet temperature.

3) When the prediction model for transmission losses associated with both the combustor/duct coupling and across the turbine itself are taken into account, the combustion noise levels from both burner rigs and full-scale engines fit a single power level prediction equation to a standard deviation of 1.7 dB. This deviation is significantly less than that experienced when the same data are compared with currently available procedures. The latter comparisons are presented in Ref. 8.

Combustion Noise Spectra

1) Since the spectral shape characteristics of combustion noise are similar for all burners investigated (including both

can-type and annular geometries), it is possible to use a single normalized spectrum for general prediction purposes.

2) Expressions have been derived analytically and verified experimentally for the peak frequencies associated with combustion noise from both can-type and annular burners. For a given burner type, this peak frequency is inversely proportional to the burner volume.

3) For a given burner, the peak frequency of combustion noise (predicted and measured) is independent of burner operating condition and far-field measurement location.

4) The measured spectra from JT8D burner component rig tests are similar to the combustion noise spectra from full-scale engines, verifying the predicted result that turbine transmission losses are not a function of frequency.

Acknowledgment

The work presented in this paper was funded by the Federal Aviation Administration under Contract No. DOT-FA75WA-3663. The authors wish to express appreciation to R. S. Zuckerman, FAA Program Manager, for his constructive suggestions and guidance during the performance of this contract.

References

[1] Mathews, D. C. and Peracchio, A. A., "Progress in Core Engine and Turbine Noise Technology," AIAA Paper 74-948, Aug. 1974.

[2] Kazin, S. B. et al., "Core Engine Noise Control Program," DOT/FAA Rept. No. FAA RD-74-125, Vols. I, II, and III, Aug. 1974.

[3] Strahle, W. C. and Shivashankara, B. N., "Combustion Generated Noise in Gas Turbine Combustors," American Society of Mechanical Engineers, Paper No. 75-GT-27, March 1975.

[4] Gerend, R. P., Kumasaka, H. P., and Roundhill, J. P., "Core Engine Noise," *Progress in Astronautics and Aeronautics*, Vol. 37, edited by H. T. Nagamatsu, MIT Press, Cambridge, Mass., 1975, pp. 305-326.

[5] Grande, E., "A Review of Core Engine Noise," Ref. 4, pp. 297-304.

[6] Plett, E. G., Chiu, H. H., and Summerfield, M., "Research on Noise Generated by Ducted Air-Fuel Combustion Systems," Third Annual Report to the Office of Naval Research, ONR Contract N00014-67-A-0151-0029, June 1974.

[7] Burdsall, E. A., Brochu, F. P., et. al., "Results of Acoustic Testing of the JT8D-109 Refan Engines," NASA CR-134875, Nov. 1975.

[8] Mathews, D. C., Rekos, N. F. Jr., and Nagel, R. T., "Combustion Noise Investigation," DOT/FAA Rept. No. FAA RD-77-3, Feb. 1977.

[9] Pickett, G. F., "Core Engine Noise Due to Temperature Fluctuations Convecting Through Turbine Blade Rows," *Progress in Astronautics and Aeronautics*, Vol. 45, edited by I. R. Schwartz, MIT Press, Cambridge, Mass., 1976, pp. 589-608.

[10] Cumpsty, N. A., "Excess Noise from Gas Turbine Exhausts," American Society of Mechanical Engineers, Paper No. 75-GT-61, March 1975.

[11] Strahle, W. C., "The Convergence of Theory and Experiment in Direct Combustion Generated Noise," Ref. 9, pp. 467-482.

[12] Motsinger, R. E. and Emmerling, J. J., "Review of Theory and Methods for Combustion Noise Prediction," *Progress in Astronautics and Aeronautics*, Vol. 46, edited by I. R. Schwartz, MIT Press, Cambridge, Mass., 1976, pp. 177-194.

[13] Huff, R. G., Clark, B. J., and Dorsch, R. G., "Interim Prediction Method for Low Frequency Core Engine Noise," NASA TMX-71627, Nov. 1974.

[14] Strahle, W. C., "On Combustion Generated Noise," *Journal of Fluid Mechanics*, Vol. 49, pt. 2, 1971, pp. 399-414.

[15] Chiu, H. H. and Summerfield, M., "Theory of Combustion Noise," *Acta Astronautica*, Vol. 1, 1974, pp. 967-984.

[16] Shivashankara, B. N., Strahle, W. C., and Handley, J. C., "Evaluation of Combustion Noise Scaling Laws by an Optical Technique, *AIAA Journal*, Vol. 13, 1975, pp. 623-627.

[17] Shafer, H. J., Plett, E. G., and Summerfield, M., "Optical Evaluation of Combustion Noise Source Terms," *AIAA Journal*, Vol. 14, Sept. 1976, pp. 1163-1164.

[18] Kinsler, L. E. and Frey, A. R., *Fundamentals of Acoustics*, 2nd ed., Wiley, New York, 1962.

[19] McMahon, M. P., "Static Noise Measurement of Full Scale Jet Engines," presented at 11th National Conference on Environmental Effects on Aircraft and Propulsion Systems, Trenton, N. J., May 1974.